B III-5

TENSILE AND TORSIONAL FRACTURE OF LOW CARBON STEEL AT LIQUID NITROGEN TEMPERATURE

Takeo YOKOBORI* and Masahiro ICHIKAWA**

ABSTRACT

Mechanical, microstructural and crystallographic factors are involved convolutedly in macroscopic brittle fracture behavior of polycrystalline low carbon steel. In order to study not only the each factor separately in a simple case, but also the interactions of these factors, in this article the following investigations were made. (a)The effect on brittle fracture of stress gradient as induced by the wall thickness of torsion specimens and by the notch effect. (b)The temperature dependence of torsion fracture stress at low temperatures with the purpose of confirming the previous conclusion on fracture criterion for brittle fracture.

A theoretical consideration also has been attempted for another explanation of brittle fracture criterion and macroscopic brittle fracture path.

§1. INTRODUCTION

Mechanical, microstructural and crystallographic factors are involved convolutedly in macroscopic mechanical behavior of polycrystalline solids. Therefore, it is needed to study not only the each factor separately in a simple case, but also the interactions of these factors as clue to the understanding of macroscopic or overall mechanical behavior. For the case of brittle fracture of steel, such type of studies have been made on tensile and torsion fracture with uniform stress distribution at liquid oxygen[1] and nitrogen temperatures.[2)-5)] In the present paper the effect on such type of brittle fracture of stress gradient as induced by the wall thickness of torsion specimens and by the notch effect were studied. The temperature dependence of torsion fracture stress at low temperatures was also investigated in order to confirm the previous conclusion[5] on fracture criterion for brittle fracture.

A theoretical consideration also has been attempted for another explanation of brittle fracture criterion and macroscopic brittle fracture path.

---

* Professor of Mechanical Engineering, Tohoku University, Sendai, Japan.

** Post Graduate of Mechanical Engineering, Tohoku University, Sendai, Japan.

§2. EXPERIMENTAL

2.1. Material and specimens preparation

The two kinds of low carbon steel were used. The one was 0.04% plain carbon steel, a killed type, basic electric-furnace steel supplied in the form of hot-rolled plate 1524 × 6096 × 32 mm from a 6.3 ton steel ingot. From blanks, cut parallel to the direction of rolling, the bars with 22 mm diameter were forged. The chemical composition of the steel is given in Table 1. We denoted this material as L-steel. The other material was 0.03% plain carbon steel, electric arc furnace steel supplied in the form of hot-forged block 300 × 300 × 300 mm from 9 ton steel ingot. The bars with 25 mm diameter were forged from the block. The chemical composition of the steel is given in Table 1. We denoted this material as M-steel.

One set of the samples of L-steel were annealed at 950°C for an hour prior to the machining into the specimens with the shape as shown in Figs. 1 and 2. Then they were annealed in vacuum at 650°C for an hour for stress relief. The ferrite grain size was ASTMGSNo.7.0. We denoted this set of the specimens as LA-specimens. LA-specimens were used mainly for study of the effect of the ratio of the inner diameter to the outer diameter, D_2/D_1, of the specimens and the stress gradient on the fracture behavior.

A few samples of L-steel were given tensile strain of 10% at room temperature and were machined into the specimens with the shape as shown in Figs.1 and 2. They were held at 1050°C for 10 hours, followed by colling at cooling rate of 40°C/hr in furnace. The grain size was ASTMGSNo.2.5. LB-specimens as which we denoted them were used for studying the effect of the grain size on the torsional fracture stress of the solid, not hollow cylindrical specimen.

Samples of M-steel were annealed in vacuum at 950°C for 1 hour after the machining into the specimen with the shape as shown in Fig. 3. The ferrite grain size was ASTMGSNo.3.5. We denoted this set of the specimens as M-specimens. M-specimens were used for the study of the temperature dependence of the torsional fracture stress of the specimens with thin-walled hollow cylindrical shape (D_2/D_1=0.833), and thus fracture criterion.

2.2. Testing procedure

For LA and LB-specimens, tensile tests and torsion tests were carried out with 30 ton tensile testing machine and with 120 kgm Amsler torsion testing machine respectively, with normal slow strain rate (about 0.01/min) under liquid nitrogen temperature specimens being immersed in a container filled with liquid nitrogen.

For M-specimens, torsion tests were carried out using combined tension and torsion testing machine designed by our laboratories with a cooling chamber patterned after the design of Wessel and Olleman[6]. Torsion tests were carried out in the temperature range 20 to -196°C,

and, however, torsional fracture stress could only be obtained in the range -160 to -196°C as described in §2.3. The strain rate was about 0.1/min.

2.3 Results and discussion

The results obtained and the analysis of them are as follows:

(1) The type of torsion fracture depends on the wall thickness of the specimens. The fracture is shear type semi-brittle fracture for the specimen with a thickness larger than a critical one. On the other hand, it is cleavage type brittle fracture for the specimen with a thickness smaller than a critical one. This characteristic is shown in Fig.4. This is confirmed by metallographical examination, and also is seen in the plastic strain prior to fracture as shown in Fig.5.

(2) In the case of shear type semi-brittle torsion fracture, the mode of crack changed into cleavage brittle crack during its propagation. The shear type semi-brittle crack path follows almost along the plane normal to the specimen axis, and, on the other hand, the cleavage brittle crack path follows along a spiral plane making about 45 degrees with the specimen axis. This characteristic is seen in Fig.6.

(3) The two types of mode were observed when the shear type semi-brittle crack changes into cleavage crack during its propagation. In the first type, the shear crack changes into cleavage crack at the early stage of its propagation, and, therefore, the initial shear crack is confined to the small part of the fracture surface (Fig.7(a)). In the second type, the shear crack changes into cleavage crack at the later stage of its propagation, and thus the initial shear crack appeared as concentric circular crack (Fig. 7(b)). This characteristic is also revealed by metallographical examination (etch pit method) as shown in Fig.8. In the case of the notched specimens only the second type was observed.

(4) The fracture stress and the maximum plastic strain prior to fracture in the case of shear type semi-brittle torsion fracture increase with increase of the specimen thickness (Figs.4 and 5 and Table 2). This predicts that this type of fracture does not obey the maximum shear stress nor maximum shear strain law.

(5) In the case of the solid, not hollow specimens and the notched specimens with grain size ASTMGSNo. 7.0-2.5 and ASTMGSNo. 7.0 respectively, fracture occurred as shear type semi-brittle fracture.

(6) The torsion fracture stress of LA3-4 specimens at -196°C increased by 5% when prestrained by 32% torsional strain at room temperature.

(7) For the range of the specimen size in the present experiment, the size effect on fracture stress is negligible (Table 3). Thus, from the analysis of the results, the effect of the specimen bar thickness upon the fracture stress in the case of shear type semi-brittle torsion fracture is considered as due to the stress gradient effect.

(8) From the results (1) and (7), it may be concluded that the cleavage

fracture is retarded by the stress gradient. Therefore, it may also be the case in the notched specimens, which is not inconsistent with the present experimental results in the case of torsion fracture.

(9) On the other hand, notch cleavage brittleness was induced by triaxial tension under the tensile test (Table 3). However, in an annular notched torsion specimen, triaxial tension is zero at least in a first approximation, and, therefore, the notch cleavage brittleness does not occur in the present torsion test.

In the previous article[5] the torsional fracture stress τ_{sf} is compared with the tensile fracture stress σ_{tf}, and we were led to the conclusion that the fracture criterion for this cleavage fracture in low carbon steel does not obey the maximum tensile stress law, nor the maximum shear stress law nor the von Mises criterion. The justification in comparing them is based on the following experimental facts: Fracture in both the tensile and the torsion test are of cleavage type, and the testing temperature -196°C is thus assumed to be below the ductile-brittle transition temperature. Moreover, such metallographic features[3] observed as slip, twinning and microcracks were quite similar in both the tensile and the torsion test, and also electron microfractographical study[4] reveals no essential difference between the tensile and torsional fractures. In this article the temperature dependence of the torsional fracture has been studied to confirm the justification still more. The result is shown in Fig.9. Above -160°C fracture is of ductile type, the amount of deformation is extremely large, and, therefore, fracture stress could not be determined. Except this, the temperature dependence characteristic appears to be similar as that indicated by many previous tensile test data in literatures.[7][8] Only difference is that ductile-brittle (ductility) transition temperature is lower in torsion test than in tensile test with the low carbon steel with the similar amount of carbon and silicon and almost the same grain size, that is, Ferrite F2 (course) by Hahn et al.[7] Nevertheless, at least at -196°C we are justified in considering the tensile fracture and the torsional fracture in such low carbon steel as the same type of fracture mode in that the metallographic features[3] and electron microfractographical characteristics[4] are similar and that in both fractures fractures are of cleavage type[2] and fracture stresses are higher[2][3] than yield stresses.

Thus we may be justified in being led to the previous conclusion[5] that the tensile stress component and the shear stress component of applied stress should be involved at the same time in cleavage fracture. If any dislocation model or atomic model is responsible for the macroscopic fracture stress of this type of fracture, the model should lead to such stress criterion. A model was proposed previously.[5] On the other hand, as will be shown in §3, it is possible to show that another fracture criterion of this type is obtained by the local maximum tensile stress law using the initially cracked model.

§3. A THEORETICAL CONSIDERATION ON BRITTLE FRACTURE CRITERION AND MACROSCOPIC FRACTURE PATH

3.1. Introduction

With respect to the macroscopic cleavage fracture path the following has been observed in experiments[1)-4)] on thin-walled cylindrical specimens of low carbon steel at liquid nitrogen temperature: In tensile fracture the macroscopic fracture path is nearly perpendicular to the specimen axis, and in torsional fracture, it is oblique by about 45 degrees with the specimen axis. These macroscopic directions are almost perpendicular to the macroscopically maximum applied tensile stress component, but fracture does not obey the maximum tensile stress law as noted by Yokobori.[1)-4)] These characteristics have not yet been sufficiently explained from a unified standpoint of view. In the present article, it is attempted to explain the above-mentioned experimental facts on the macroscopic cleavage fracture path as well as fracture criterion of this type in polycrystalline low carbon steel.

3.2. A proposed model of formation of the macroscopic fracture path

In our tensile and torsional tests at -196°C[2)-5)] fracture of low carbon steel is completely cleavage and is initiated by cleavage microcracks. Based on these experimental facts, we propose the following model: A cleavage microcrack $P_o'P_o$ is formed in the grain G_o and is stopped at grain boundaries as shown in Fig.10. Crack propagation in the right hand direction only will be considered, since that in the opposite direction may be treated similarly. When the applied stress reaches some critical stress, this microcrack gets over the grain boundary and propagates in the grain G_1 along a cleavage plane P_oP_1 of the grain G_1. This stage is called the 1st stage. Next, the crack propagates further in the grain G_2 along a cleavage plane P_1P_2 of the grain G_2. This stage is called the 2nd stage.*** In the similar way, the crack continues to propagate through the 3rd stage, the 4th stage----. It is assumed that the crack does not change its path from one cleavage plane to another in one and the same grain. This is based on the observation that the cleavage fracture path is generally consisted of straight segments of about a grain diameter in length.

Let n be an arbitrary positive integer. The direction of propagation at the nth stage, i.e, that of the segment $P_{n-1}P_n$ must satisfy the condition that it is the direction of a cleavage plane of the grain

*** So far as the direction of propagation of the initial (primary) microcrack, that is, the direction of the secondary crack, is concerned, the studies have been made by Erdogan et al[13)] and Schröder et al[14)] for a slit crack and an elliptic crack respectively. On the other hand, Cotterell[15)] treated mainly on the direction of crack propagation at an arbitrary instant.

G_n. We call it the crystallographic condition. This alone cannot determine the direction of the segment $P_{n-1}P_n$ uniquely, since the body-centered cubic lattice has three cleavage planes perpendicular each other. Another condition required in addition to the crystallographic condition must be one connected with mechanical state of a specimen. We call it the mechanical condition. Some plausible mechanical conditions may be considered. Among them we adopt one that the segment $P_{n-1}P_n$ is in accordance with the plane on which tensile stress has the maximum, i,e, the plane of the maximum tensile stress, unless any obstacle by other factors is present. Thus, combining both the crystallographic and the mechanical conditions, it is assumed that the segment $P_{n-1}P_n$ is in accordance with one of cleavage planes of the grain G_n on which the tensile stress is the largest of tensile stresses on cleavage planes.

3.3. The essential nature of the mechanical condition

In this section, we consider an isotropic, homogeneous solid, that is, an ideal case in which the plane of the maximum tensile stress at the tip is always in accordance with one of cleavage planes of an adjacent grain. By considering such an ideal case, the essential nature of the mechanical condition adopted in §3.2 will be understood.

Firstly, let's consider a slit crack of length 2C in an infinite elastic solid subject to both tensile stress σ and shear stress τ at infinity as shown in Fig.11. Let σ_θ be normal stress on a plane OP at a point P in the neighborhood of the crack tip O. σ_θ is given as:[9)10)]

$$\sigma_\theta = \frac{1}{2}\sqrt{\frac{C}{2r}}\cos\frac{\theta}{2}\left[\sigma(1+\cos\theta)-3\tau\sin\theta\right], \qquad (1)$$

where Θ is the angle between the plane OP and the positive x direction and r is distance between the point P and the tip O such that $r \ll C$. Let Θ_m be Θ at which σ_θ has the maximum for a fixed value of r. Θ_m is obtained by solving the equation $\partial\sigma_\theta/\partial\Theta = 0$ as:

$$\Theta_m = \mp\cos^{-1}\left[\frac{3\tau^2+\sigma\sqrt{8\tau^2+\sigma^2}}{9\tau^2+\sigma^2}\right], \qquad (2)$$

where the negative and positive signs are for $\tau \geqq 0$ and $\tau \leqq 0$ respectively, and values of arc cosine are to be taken between O and π. Substituting Eq. (2) into Eq. (1), $\sigma_{\theta max}$ the maximum of σ_θ is obtained as:

$$\sigma_{\theta max} = \sqrt{\frac{C}{2r}}\left[\frac{24\tau^4+12\tau^2\sigma^2+\sigma^4+\sigma(8\tau^2+\sigma^2)^{\frac{3}{2}}}{2(9\tau^2+\sigma^2)}\right]^{\frac{1}{2}}. \qquad (3)$$

It is to be noted that these results are valid for $\sigma < 0$ as well as for $\sigma \geqq 0$.

Now, we consider crack propagation under uni-axial tension. In Fig.12 the y axis is taken in parallel with the direction of the applied tensile stress P, or the specimen axis. When propagation has finished the (n-1) th stage, the macroscopic fracture path is consisted of n segments P'_oP_o, P_oP_1, -------, $P_{n-2}P_{n-1}$. Let ϕ_o, ϕ_1, -----, ϕ_{n-1} be the angles between the positive x direction and the segments P'_oP_o, P_oP_1, ---- $P_{n-2}P_{n-1}$, respectively. Also, let Θ_m be the angle between the plane of the maximum tensile stress at the tip P_{n-1} and the prolongation of the segment $P_{n-2}P_{n-1}$. Strictly, Θ_m is dependent on all of ϕ_o, ϕ_1 ---- ϕ_{n-1}. In the present article, however, we assume in a first approximation that Θ_m is a function of ϕ_{n-1} only. Then, Θ_m is obtained by substituting $\sigma = P\cos^2\phi_{n-1}$ and $\tau = P\cos\phi_{n-1}\sin\phi_{n-1}$ into Eq.(2) as:

$$\Theta_m = \mp\cos^{-1}\left[\frac{3\tan^2\phi_{n-1}+\sqrt{8\tan^2\phi_{n-1}+1}}{9\tan^2\phi_{n-1}+1}\right], \qquad (4)$$

where the negative and positive signs are for $0 \leqq \phi_{n-1} \leqq \frac{\pi}{2}$ and $-\frac{\pi}{2} \leqq \phi_{n-1} \leqq 0$, respectively. Since we are treating such an ideal case in which the plane of the maximum tensile stress is always in accordance with one of cleavage planes, the angle between the direction of propagation at the nth stage, i,e, that of the segment $P_{n-1}P_n$ and the positive x direction, ϕ_n, is given as:

$$\phi_n = \phi_{n-1} + \Theta_m. \qquad (5)$$

The calculated values of ϕ_n are plotted against ϕ_{n-1} in Fig.13. The curve for $\phi_{n-1} < 0$ is not shown. ϕ_n is an odd function of ϕ_{n-1}.

Next, let's consider a problem of getting ϕ_1, ϕ_2, ----, ϕ_n, ---- when ϕ_o is given arbitrarily. This problem can be solved by the following graphical method most conviniently: In Fig.14 the ϕ_n curve is shown as in Fig.13. The straight line denotes $\phi_n = \phi_{n-1}$. Draw a normal to the ϕ_{n-1} axis at the point $(\phi_o, 0)$, and let the point A be the intersection of this with the ϕ_n curve. Then, draw from A a parallel with the ϕ_{n-1} axis and let B be the intersection of this with the line $\phi_n = \phi_{n-1}$. Draw from B a normal to the ϕ_{n-1} axis, and then ϕ_1 will be obtained as the ϕ_{n-1} coordinate of the intersection of this with the ϕ_{n-1} axis. In the similar way, ϕ_2, ϕ_3, ---- can be found. Applying this method to various values of ϕ_o, the following general results are obtained. When ϕ_o is 0° or 60°, $\phi_1 = \phi_2 = \text{----} = 0^\circ$, i,e, the direction of propagation during each stage is always parallel to the x axis. When ϕ_o is neither 0° nor 60°,

$$(i) \quad \lim_{n\to\infty}\phi_n = 0^\circ \qquad (6)$$

(ii) $\phi_{n-1}\phi_n < 0 \quad (n \geq 2)$. (7)

Eq.(6) implies that the final direction of propagation is parallel with the x axis. Practically, this steady state is attained at a rather early stage. For instance, $\phi_{30} = 0.5^\circ$ when $\phi_0 = 10^\circ$. Eq.(7) implies that deviation of the direction of propagation from that of the x axis at two successive stages are opposite sense each other, and therefore cancel partly. For example, $\phi_{29} + \phi_{30} = 0.05^\circ$ when $\phi_0 = 10^\circ$. From these results, it may be concluded that the macroscopic fracture path under tension in the ideal case is perpendicular to the specimen axis independent of the orientation of an initial microcrack.

Next, we consider crack propagation under torsion in this ideal case. The case of simple shear will be treated. In Fig.15 the x and y axes are taken in parallel with the directions of the applied shear stress S. The u axis makes 45° with the x axis and therefore perpendicular to the macroscopically maximum applied tensile stress. When propagation has finished the (n-1)th stage, the macroscopic fracture path is consisted of n segments $P_0'P_0$, P_0P_1, ----, $P_{n-2}P_{n-1}$. Let $\psi_0, \psi_1, ----, \psi_{n-1}$ be the angles between the positive u direction and the segments $P_0'P_0$, P_0P_1, ----, $P_{n-2}P_{n-1}$, respectively. Also, let Θ_m be the angle between the plane of the maximum tensile stress at the tip P_{n-1} and the prolongation of the segment $P_{n-2}P_{n-1}$. Substituting $\sigma = S\cos 2\psi_{n-1}$ and $\tau = S\sin 2\psi_{n-1}$ into Eq.(2), Θ_m is obtained as:

$$\left.\begin{aligned} \theta_m &= \mp\cos^{-1}\left[\frac{3\tan^2 2\psi_{n-1} + \sqrt{8\tan^2 2\psi_{n-1}+1}}{9\tan^2 2\psi_{n-1}+1}\right] \quad \text{for } 0 \leqq |\psi_{n-1}| \leqq \frac{\pi}{4} \\ \theta_m &= \mp\cos^{-1}\left[\frac{3\tan^2 2\psi_{n-1} - \sqrt{8\tan^2 2\psi_{n-1}+1}}{9\tan^2 2\psi_{n-1}+1}\right] \quad \text{for } \frac{\pi}{4} \leqq |\psi_{n-1}| \leqq \frac{\pi}{2} \end{aligned}\right\} \quad (8)$$

where the negative and positive signs are for $\psi_{n-1} \geqq 0$ and $\psi_{n-1} \leqq 0$ respectively. The angle ψ_n between the direction of propagation at the nth stage and the positive u direction is:

$$\psi_n = \psi_{n-1} + \theta_m . \quad (9)$$

The calculated values of ψ_n are plotted against ψ_{n-1} in Fig.16. The curve for $\psi_{n-1} < 0$ is not shown. ψ_n is an odd function of ψ_{n-1}.

The macroscopic fracture path can be studied by the similar method as described in the case of tension. The results are as follows: When $\psi_0 = 0^\circ$, $\psi_1 = \psi_2 = ----\ 0^\circ$, i,e, the direction of propagation during each stage is always parallel with the u axis. When ψ_0 is not 0°,

(i) if $\psi_0 > 0^\circ$, $\lim_{n\to\infty}\psi_{2n} = 30^\circ$ and $\lim_{n\to\infty}\psi_{2n+1} = -30^\circ$
if $\psi_0 < 0^\circ$, $\lim_{n\to\infty}\psi_{2n} = -30^\circ$ and $\lim_{n\to\infty}\psi_{2n+1} = 30^\circ$ (10)

(ii) $\psi_{n-1}\psi_n < 0 \quad (n \geq 1)$. (11)

Eq.(10) implies that the final path of fracture follows a zigzag line consisting of segments oblique by 30° and -30° with the positive u direction alternatively. Therefore, the overall, macroscopic direction of the fracture path in the steady state is parallel with the u axis. Practically this steady state is attained at a rather early stage. For example, $\psi_2 = 30.5^\circ$, $\psi_3 = -29.9^\circ$ and $\psi_2 + \psi_3 = 0.6^\circ$ when $\psi_0 = 10^\circ$. The meaning of Eq.(11) is similar to that of Eq.(7). From these results, it may be concluded that the macroscopic fracture path under torsion in the ideal case makes 45° with the specimen axis independent of the orientation of an initial microcrack. The present treatment suggests that the mechanical condition adopted in §3.2 has such an essential nature as makes the macroscopic fracture path perpendicular to and oblique by 45° with the specimen axis in the case of tension and in that of torsion, respectively.

3.4 The macroscopic fracture path

(1) The case of uni-axial tension

In this section, we consider the macroscopic fracture path in polycrystalline solids, in which the plane of the maximum tensile stress at the crack tip does not accord with any of cleavage planes generally.

Let's consider the nth stage of crack propagation. In Fig.17 the coordinates system is taken in the same way as in Fig.12. Since the present treatment is two-dimensional, it follows that there exist two cleavage planes passing the tip P_{n-1} (C_1C_3 and C_2C_4) of the grain G_n which are perpendicular each other. Therefore, four directions, $P_{n-1}C_1$, $P_{n-1}C_2$, $P_{n-1}C_3$ and $P_{n-1}C_4$, satisfy the crystallographic condition at the same time. Of course, some of these four directions may not belong to the interior of the grain G_n. For simplicity, however, we assume that all the directions passing the tip P_{n-1} belong to the interior of the grain G_n. This assumption will be discussed in §3.6. Thus, it follows that propagation at the nth stage occurs along one of planes $P_{n-1}C_1$, $P_{n-1}C_2$, $P_{n-1}C_3$ and $P_{n-1}C_4$ on which σ_θ is the largest of σ_θ on the four planes. On the other hand, crystallographic orientations of grains in a specimen have generally a random distribution. From this and the above assumption, it follows that all the planes passing the tip P_{n-1} have equal probability of being a cleavage plane. Then, the direction of propagation at the nth stage is located in an angular region of $\pi/2$ in which σ_θ are larger than σ_θ in the remainder region. We express this region by $\alpha(\phi_{n-1}) < \phi < \beta(\phi_{n-1})$.

Here, ϕ is measured from the x axis in anti-clockwise direction. $\alpha(\phi_{n-1})$ and $\beta(\phi_{n-1})$ are determined by the following conditions:

$$\sigma_\theta\left(\alpha(\phi_{n-1})<\phi<\beta(\phi_{n-1})\right) > \sigma_\theta\left(\phi<\alpha(\phi_{n-1}) \text{ and } \phi>\beta(\phi_{n-1})\right) \tag{12}$$

$$\beta(\phi_{n-1}) - \alpha(\phi_{n-1}) = \frac{\pi}{2} . \tag{13}$$

σ_θ in the case of tension is obtained by substituting $\sigma = P\cos^2\phi_{n-1}$ and $\tau = P\cos\phi_{n-1}\sin\phi_{n-1}$ and $\Theta = \phi - \phi_{n-1}$ into Eq.(1) as:

$$\sigma_\theta \propto \cos\frac{\phi-\phi_{n-1}}{2}\left[1+\cos(\phi-\phi_{n-1})-3\tan\phi_{n-1}\sin(\phi-\phi_{n-1})\right] . \tag{14}$$

The calculated values of $\alpha(\phi_{n-1})$ and $\beta(\phi_{n-1})$ by Eqs.(12),(13) and (14) are plotted in Fig.18. $1/2\left\{\alpha(\phi_{n-1})+\beta(\phi_{n-1})\right\}$ is also shown. It may be noticed that $1/2\left\{\alpha(\phi_{n-1})+\beta(\phi_{n-1})\right\}$ is almost equal to ϕ_n in Fig.13. This means that the direction of the plane of the maximum tensile stress at the tip P_{n-1} is almost the middle of the region $\alpha(\phi_{n-1}) < \phi < \beta(\phi_{n-1})$.

Now, let's consider crack propagation initiated by a microcrack with an arbitrary value of ϕ_0. Let $F_1(\phi)$ be the probability density function of the direction of propagation at the 1st stage. From the above argument, $F_1(\phi)$ may be expressed as:

$$F_1(\phi) = \begin{cases} 1/90 & \alpha(\phi_0)<\phi<\beta(\phi_0) \\ 0 & \phi<\alpha(\phi_0) \text{ or } \phi>\beta(\phi_0) \end{cases} . \tag{15}$$

Propagation at the 2nd stage must be considered for all the directions of propagation at the 1st stage with weight proportional to $F_1(\phi)$. Therefore, $F_2(\phi)$ the probability density function of the direction of propagation at the 2nd stage becomes as follows:

$$F_2(\phi) = \int_{-180}^{180} F_1(\omega) f(\phi,\omega)\, d\omega , \tag{16}$$

where

$$f(\phi,\omega) = \begin{cases} 1/90 & \alpha(\omega)<\phi<\beta(\omega) \\ 0 & \phi<\alpha(\omega) \text{ or } \phi>\beta(\omega) \end{cases} , \tag{17}$$

and ω is a variable of integration. Generally, $Fn(\phi)$ the probability density function of the direction of propagation at the nth stage is expressed with $F_{n-1}(\phi)$ that of the (n-1)th stage as:

$$Fn(\phi) = \int_{-180}^{180} F_{n-1}(\omega) f(\phi,\omega)\, d\omega . \tag{18}$$

Calculation of $Fn(\phi)$ was performed by approximating the curves of $\alpha(\phi_{n-1})$ and $\beta(\phi_{n-1})$ in Fig.18 by stepwise ones with interval of 5° as shown in Fig.19, since precise calculation is very complex. Among the results, that for $\phi_0 = 22.5°$ is shown in Fig.20. Here ϕ_n^* is the mean value of the direction of propagation at the nth stage calculated by the following formula:

$$\phi_n^* = \int_{-180}^{180} \phi F_n(\phi)\, d\phi . \tag{19}$$

Also, F_n^+ and F_n^- are:

$$\left.\begin{aligned} F_n^+ &= \int_{\phi\geq 0} F_n(\phi)\, d\phi \\ F_n^- &= \int_{\phi\leq 0} F_n(\phi)\, d\phi . \end{aligned}\right\} \tag{20}$$

The results for other values of ϕ_0 showed the similar trend as that shown in Fig.20.

From this calculation, the followings may be concluded. When $\phi_0 =$ 0° or 60°, $F(\phi)$ during each stage is always symmetrical with respect to $\phi = 0°$. When ϕ_0 is neither 0° nor 60°,

(i) As $n\to\infty$, $Fn(\phi)$ becomes exactly symmetrical with respect to $\phi =$ 0°. Practically, symmetry is attained at a rather early stage as the present calculation shows.

(ii) The deviation of $Fn(\phi)$ from exact symmetry at two successive stages are opposite in direction and therefore cancel each other partly.

Thus, the present theory predicts that the macroscopic fracture path under tension is perpendicular to the specimen axis independent of the orientation of an initial microcrack.

(2) The case of torsion

Next, we consider the case of torsion. The coordinates system is taken in the same way as in Fig.15. Let ψ_{n-1} be the angle between the direction of propagation at the (n-1)th stage and the positive u direction. The direction of propagation at the nth stage is located in an angular region of $\pi/2$. We express this region by $\xi(\psi_{n-1}) < \psi < \eta(\psi_{n-1})$. Here, ψ is measured from the u axis in anti-clockwise direction. $\xi(\psi_{n-1})$ and $\eta(\psi_{n-1})$ are calculated in the quite similar way as in the case of tension. The results are shown in Fig.21. At such ψ_{n-1} for which $\xi(\psi_{n-1}) > \eta(\psi_{n-1})$, the region $\xi(\psi_{n-1}) < \psi < \eta(\psi_{n-1})$ should be understood as the regions $\xi(\psi_{n-1}) < \psi < 180°$ and $-180° < \psi < \eta(\psi_{n-1})$. $1/2\left\{\xi(\psi_{n-1})+\eta(\psi_{n-1})\right\}$ is almost equal to ψ_n in Fig.16 as in the case of tension. In the case of torsion, however, $|\xi(\psi_{n-1})|$ and $|\eta(\psi_{n-1})|$ exceed 90° for some values of ψ_{n-1} between -90° and 90° and therefore the curve for $|\psi_{n-1}| > 90°$ must be shown. Another characteristic

which was not seen in the case of tension is that there exist such parts where $\sigma_\theta \leqq 0$ in the region $\xi(\psi_{n-1}) < \psi < \eta(\psi_{n-1})$. These parts are marked by hatching in Fig.21. If the direction of propagation falls in such parts, successive propagation will not be possible. In the present treatment, however, we do not consider such a phenomenon, and so the hatched parts are omitted from consideration. Now, let $Gn(\psi)$ and ψ_n^* be the probability density function and the averaged direction angle of propagation at the nth stage. These can be calculated in the similar way as in the case of tension using the approximated functions of $\xi(\psi_{n-1})$ and $\eta(\psi_{n-1})$ as shown in Fig.22. Among the results, that for $\psi_0 = 22.5^\circ$ is shown in Fig.23. Here, G_n^+ and G_n^- have the quite similar meaning as F_n^+ and F_n^- in the case of tension, respectively. For other values of ψ_0, the similar trend was found. Therefore, the followings may be concluded: When $\psi_0 = 0^\circ$, $G(\psi)$ during each stage is always symmetrical with respect to $\psi = 0^\circ$. When $\psi_0 \neq 0^\circ$,

(i) As $n \to \infty$, $Gn(\psi)$ becomes exactly symmetrical with respect to $\psi = 0^\circ$. Practically, symmetry can be attained at a rather early stage as the present calculation shows.

(ii) The deviation of $Gn(\psi)$ from exact symmetry at two successive stages are opposite in direction and therefore cancel each other partly.

Thus, the present theory predicts that the macroscopic fracture path under torsion is oblique by 45° with the specimen axis independent of the orientation of an initial microcrack.

3.5 The fracture criterion

In this section, we will propose a fracture criterion based on the proposed model in §3.2. We assume fracture stress is not determined by formation of cleavage microcracks but by propagation of those, since cleavage microcracks are observed before fracture.[7)3)] Now, we assume that if propagation at the 1st stage is initiated, the subsequent propagation can occur without any increase in the applied stress. Thus, the fracture stress is assumed to be the stress required for propagation at the 1st stage, i.e., initiation of the secondary crack from the initial crack. Further we assume that propagation at the 1st stage occurs when $\sigma_{\theta max}$, the maximum of stresses σ_θ at points with distance r_c from the tip of an initial microcrack reaches a certain critical value K, i,e, when the condition

$$\sigma_{\theta max} = K \tag{21}$$

is fulfiled.

Firstly, let's consider the case of tension. The coordinates system is taken in the same way as in Fig.12. Let ϕ_0 be the angle between a microcrack and the positive x direction. $\sigma_{\theta max}$ is obtained by substituting $\sigma = P\cos^2\phi_0$ and $\tau = P\cos\phi_0\sin\phi_0$ into Eq.(3) as:

$$\sigma_{\theta max} = P\sqrt{\frac{C}{2r_c}}\cos^2\phi_0\left[\frac{24\tan^4\phi_0+12\tan^2\phi_0+1+(8\tan^2\phi_0+1)^{\frac{3}{2}}}{2(9\tan^2\phi_0+1)}\right]^{\frac{1}{2}}. \tag{22}$$

Let $P_f(\phi_0)$ be the stress required for propagation of a microcrack with orientation ϕ_0. From Eqs.(21) and (22), $P_f(\phi_0)$ is obtained as:

$$P_f(\phi_0) = K\sqrt{\frac{2r_c}{C}}\frac{1}{\cos^2\phi_0}\left[\frac{24\tan^4\phi_0+12\tan^2\phi_0+1+(8\tan^2\phi_0+1)^{\frac{3}{2}}}{2(9\tan^2\phi_0+1)}\right]^{-\frac{1}{2}}. \tag{23}$$

Particularly, $P_f(0) = K\sqrt{\frac{2r_c}{C}}$.

The calculated values of $P_f(0)/P_f(\phi_0)$ by Eq.(23) are plotted against ϕ_0 in Fig.24. It is seen that the microcrack with the orientation of $\phi_0 \fallingdotseq 20^\circ$ is weakest. Now, let P_{fr} be the tensile fracture stress of a specimen. Since a specimen contains microcracks with random orientations, P_{fr} is determined by the minimum of $P_f(\phi_0)$. Therefore

$$P_{fr} = \frac{K}{1.03}\sqrt{\frac{2r_c}{C}}. \tag{24}$$

Next let's consider the case of torsion. The coordinates system is taken in the same way as in Fig.15. Let $S_f(\psi_0)$ be the stress required for propagation of a microcrack which makes an angle ψ_0 with the positive u direction. Then, $S_f(\psi_0)$ is obtained in the similar way as in the case of tension as:

$$S_f(\psi_0) = K\sqrt{\frac{2r_c}{C}}\frac{1}{|\cos 2\psi_0|}\left[\frac{24\tan^4 2\psi_0+12\tan^2 2\psi_0+1 \mp (8\tan^2 2\psi_0+1)^{\frac{3}{2}}}{2(9\tan^2 2\psi_0+1)}\right]^{-\frac{1}{2}}, \tag{25}$$

where the negative and positive signs are for $\frac{\pi}{4} \leqq |\psi_0| \leqq \frac{\pi}{2}$ and $0 \leqq |\psi_0| \leqq \frac{\pi}{4}$, respectively. Particularly, $S_f(0) = K\sqrt{\frac{2r_c}{C}}$. The calculated values of $S_f(0)/S_f(\psi_0)$ by Eq.(25) are plotted against ψ_0 in Fig.25. It is seen that the microcrack with the orientation of $\psi_0 \fallingdotseq 30^\circ$ is weakest. Now, S_{fr} the torsional fracture strength of a specimen is obtained as the minimum of $S_f(\psi_0)$ as:

$$S_{fr} = \frac{K}{1.3}\sqrt{\frac{2r_c}{C}}. \tag{26}$$

According to the present theory, the ratio of the torsional fracture stress to the tensile fracture stress is calculated from Eqs.(24) and (26) as:

$$S_{fr}/P_{fr} = 0.79. \tag{27}$$

The present theory is implicitly based on the assumption that the plane

of the maximum tensile stress near the tip of a microcrack is in accordance with a cleavage plane. This will not be satisfied in general. So, S_{fr} and P_{fr} may be effected by this factor. However, the ratio S_{fr}/P_{fr} will not be changed seriously, since effect of this factor on S_{fr} and P_{fr} are considered to be of the same degree.

On the other hand, Priestner and Louat[11] has proposed the following condition for propagation of a crack subject to both normal stress σ and shear stress τ as shown in Fig.11:

$$\sigma^2 + \tau^2 = \frac{2E\gamma}{\pi(1-\nu^2)C} , \tag{28}$$

where E is Young's modulus, γ is the surface energy, ν is Poisson's ratio and C is the half length of a crack. This condition is an extension of the Griffith[12] energy condition. However, it is to be noticed that Eq.(28) is based on the assumption that a crack expands in the direction of the prolongation of the crack axis.

Now, if Eq.(28) is used instead of Eq.(21), $P_f(\phi_o)$ becomes as follows:

$$P_f(\phi_o) = \sqrt{\frac{2E\gamma}{\pi(1-\nu^2)C}} \frac{1}{\cos\phi_o} . \tag{29}$$

Particularly, $P_f(O) = \sqrt{\frac{2E\gamma}{\pi(1-\nu^2)C}}$. Similarly, $S_f(\psi_o)$ and $S_f(O)$ are:

$$S_f(\psi_o) = S_f(0) = \sqrt{\frac{2E\gamma}{\pi(1-\nu^2)C}} . \tag{30}$$

The calculated values of $P_f(O)/P_f(\phi_o)$ and $S_f(O)/S_f(\psi_o)$ by Eqs.(29) and (30) are shown in Figs.24 and 25 respectively. P_{fr} and S_{fr} are obtained as:

$$P_{fr} = S_{fr} = \sqrt{\frac{2E\gamma}{\pi(1-\nu^2)C}} . \tag{31}$$

Therefore, according to the Priestner and Louat's theory the ratio of the torsional fracture stress to the tensile fracture stress becomes as follows:

$$S_{fr}/P_{fr} = 1.0 . \tag{32}$$

3.6 Discussion

The present theory predicts that the macroscopic cleavage fracture path in polycrystalline solids is perpendicular to and oblique by 45 degrees with the specimen axis in tensile fracture and in torsion fracture, respectively. This is in good agreement with the experimental results[1)-4)] mentioned in §3.1.

The theory predicts that the direction of the macroscopic fracture path is independent of the orientation of an initial microcrack. This is important in the sense that the macroscopic fracture path is determined only by such a continuum mechanical aspect, whatever dislocation mechanism or whatever micromechanism may be as the microcrack formation one.

Another important prediction of the present theory is that the macroscopic fracture path is not affected essentially by such a random statistical factor as crystallographic orientations of grains. This may be understood from comparison of the result of §3.4 with that of §3.3. In the theory, the shapes of grain boundaries are not taken into account. If this is done, probability of existence of a cleavage plane at the crack tip will be dependent on the direction, and so the shape of the curves of Fn (ϕ) and Gn(ψ) will be somewhat modified. However, such modification will not affect the essential result of the theory, since the factor of shapes of grain boundaries is a rondom statistical one just as the factor of crystallographic orientations of grains is.

As for the fracture criterion, our theory indicates that the ratio of the torsional fracture stress to the tensile fracture stress is about 0.79. This is near to the experimental ratio[2)-4)] which is ranging from 0.55 to 0.82 depending on grain size. On the other hand, the ratio becomes 1.0 according to the Priestner and Louat's theory.

3.7 Conclusions

Using elastic continuum mechanics, the study has been carried out on the problems concerning fracture criterion and macroscopic cleavage fracture path in polycrystalline low carbon steel. The conclusions are as follows:

(1) Assuming (macroscopic) fracture stress is determined by the initiation of the secondary crack from the tip of the initial (primary) crack already initiated in the body, fracture criterion for this type of cleavage fracture was obtained. The theory indicates that the ratio of torsional fracture strength to the tensile fracture strength is about 0.79, which seems to be near the value in our experiments.

(2) The proposed theory predicts that the macroscopic fracture path is perpendicular to, and oblique by 45 degrees with the specimen axis in tension specimen and in torsion specimen respectively for this type of brittle fracture. This indication is in good agreement with the experiments.

(3) Since the length of the initial crack, 2C is considered equal to the grain diameter , Eqs.(24) and (26) mean that the fracture stress is proportional to the inverse square root of the grain diameter, which is in agreement with the experiments.

(4) The theory predicts that the macroscopic fracture path is independen of the orientation of an initial microcrack. It is very important in that the macroscopic fracture path is determined only by such a continuum mechanical aspect, whatever dislocation mechanism or whatever micromechanism may be as the microcrack initiation one.

4. CONCLUSIONS

The results obtained and the analysis of them are as follows:
(1) The type of torsion fracture depends on the wall thickness of the specimens. The fracture is shear type semi-brittle fracture for the specimen with a thickness larger than a critical one. On the other hand, it is cleavage type brittle fracture for the specimen with a thickness smaller than a critical one.
(2) In the case of shear type semi-brittle torsion fracture, the mode of crack changed into cleavage brittle crack during its propagation. The shear type semi-brittle crack path follows almost along the plane normal to the specimen axis, and, on the other hand, the cleavage brittle crack path follows along a spiral plane making about 45 degrees with the specimen axis.
(3) The two types of mode were observed when the shear type semi-brittle crack changes into cleavage crack during its propagation. In the first type, the shear crack changes into cleavage crack at the early stage of its propagation, and, therefore, the initial shear crack is confined to the small part of the fracture surface. In the second type, the shear crack changes into cleavage crack at the later stage of its propagation, and thus the initial shear crack appeared as a concentric circular crack. In the case of the notched specimens only the second type was observed.
(4) The fracture stress and the maximum plastic strain prior to fracture in the case of shear type semi-brittle torsion fracture increase with increase of the specimen thickness. This predicts that this type of fracture does not obey the maximum shear stress nor maximum shear strain law.
(5) In the case of the solid, not hollow specimens and the notched specimens with grain size ASTMGSNo.7.0-2.5 and ASTMGSNo.7.0 respectively, fracture occurred as shear type semi-brittle fracture.
(6) The torsion fracture stress at -196°C increased by 5% when prestrained by 32% torsion strain at room temperature.
(7) For the range of the specimen size in the present experiment, the size effect on fracture stress is negligible. Thus, from the analysis of the results, the effect of the specimen wall thickness upon the fracture stress in the case of shear type semi-brittle torsion fracture is considered as due to the stress gradient effect.
(8) From the results (1) and (7), it may be concluded that the cleavage fracture is retarded by the stress gradient. Therefore, it may also be the case in the notched specimens, which is not inconsistent with the present experimental results in the case of torsion fracture.
(9) On the other hand, notch cleavage brittleness was induced by triaxial tension under the tensile test (Table 3). However, in an annular notched torsion specimen, triaxial tension is zero at least in a first approximation, and, therefore, the notch cleavage brittleness does not occur in the present torsion test.
(10) The temperature dependence of the torsional fracture has been studied to confirm the justification in comparing the tensile and torsion fracture

stress of low carbon steel at -196°C. The result was proved to be reasonable.

On the other hand, it is possible to obtain another theoretical explanation for fracture criterion and macroscopic cleavage fracture path mentioned above. Using elastic continuum mechanics, the study has been carried out on the problems concerning fracture criterion and the macroscopic cleavage fracture path in polycrystalline low carbon steel. The following conclusions are obtained.
(11) Assuming (macroscopic) fracture stress is determined by the initiation of the secondary crack from the tip of the initial (primary) crack already initiated in the body, fracture criterion for this type of fracture was obtained. The theory indicates that the ratio of torsional fracture strength to the tensile fracture strength is about 0.79, which seems to be near the value in our experiments.
(12) The proposed theory predicts that the macroscopic fracture path is perpendicular to, and oblique by 45 degrees with the specimen axis in tensile fracture and in torsion fracture respectively for this type of brittle fracture. This indication is in good agreement with the experiments.
(13) The proposed theory also predicts that the fracture stress is proportional to the inverse square root of the grain diameter, which is in agreement with the experiments.
(14) The theory predicts that the macroscopic fracture path is independent of the orientation of an initial microcrack. It is very important in that the macroscopic fracture path is determined only by such a continuum mechanical aspect, whatever dislocation mechanism or whatever micromechanism may be as the microcrack initiation one.

ACKNOWLEDGEMENT

The study was a part of the research project of the 129 Committee (The Strength, Fracture and Fatigue Committee) of the Japan Society for Promotion of Science. The authors acknowledge the supply and preparation of the material by Drs. H. Shimoda and J. Watanabe, Head and Staff, respectively, of Central Research Laboratory, Nippon Steel Works Hokkaido.

REFERENCES

1) T. Yokobori, H. Hamamoto and A. Otsuka, Nature, Vol.181, No.4623, 1958, P.1719; Tech. Rep. Tohoku Univ., Vol.24, 1960, P.126.
2) T. Yokobori and A. Otsuka, Proc. 1st. Intern. Congr. on Exper. Mech., Pergamon Press, 1963, P.353.
3) T. Yokobori and M. Hanzawa, Tech. Rep. Tohoku Univ., Vol.28, 1964, P.141.
4) T. Yokobori, T. Takahashi and H. Kishimoto, J. Aust. Inst. Metals, Vol.8, 1963, P.184; Tech. Rep. Tohoku Univ., Vol.28, 1964, P.153

5) T. Yokobori, Tech. Rep. Tohoku Univ., Vol.28, 1964, P.167.
6) E. T. Wessel and R. D. Olleman, ASTM Bull., No.187, 1953, P.56.
7) G. T. Hahn, B. L. Averbach, W. S. Owen and M. Cohen, Fracture, B. L. Averbach et al Ed., MIT, 1959, P.91.
8) E. T. Wessel, Proc. ASTM. STP No.283, 1960, P.99.
9) G. R. Irwin, Encyclopedia of Physics, Springer Verlag, Vol.6, 1958, P.551.
10) M. L. Williams , J. Appl. Mech., Vol.24, 1957, P.109.
11) R. Priestner and N. Louat, Act. Met., Vol.11, 1963, P.195.
12) A. A. Griffith, Phil. Trans. Roy. Soc. London, Vol.221, 1921, P.163.
13) F. Erdogan and G. C. Sih, Trans. ASME., J. Basic. Eng., Vol.85, Ser. D, 1963, P.519.
14) K. Schröder, P. Packman and V. Weiss, Act. Met., Vol.12, 1964, P.1455.
15) B. Cotterell, Int. Journal of Fracture Mechanics, Vol.1, No.2 , 1965, P.96.

Table 1. Chemical Analysis of Materials (percent)

Material Symbol	C	Si	Mn	P	S	Ni	Cr	Mo
L-steel	0.04	0.01	0.15	0.027	0.023	0.15	0.02	0.05
M-steel	0.03	0.01	0.04	0.003	0.016	0.01	0.01	

Table 2. Torsion Test Results

Specimen NO.	Wall Thickness (t mm)	Ratio of Inner Diameter to Outer Diameter (D_2/D_1)	Fracture Stress* (τ kg/mm^2)	Shear Strain prior to Fracture** (γ)	Fracture Type
LA 1	0.5	0.9	——	0.22	Cleavage type
LA 2			49.5	0.21	
LA 3	1.0	0.8	56.1	0.57	Cleavage type
LA 4			55.1	0.58	
LA 5	1.5	0.7	57.4	1.99	Shear type
LA 6			60.0	1.93	
LA 7	2.0	0.6	61.9	2.43	Shear type
LA 8			61.1	2.14	
LA 9	2.5	0.5	59.8	2.01	Shear type
LA 10			61.9	2.34	
LA 11	3.0	0.4	63.5	2.68	Shear type
LA 12			61.9	2.42	
LA 13	3.5	0.3	59.7	2.18	Shear type
LA 14			62.0	2.57	
LA 16	5.0	0	63.8	3.70	Shear type
LA 17			63.8	3.68	
LA 25			62.4	3.72	
LB 1			54.3	2.26	
LA 26	Notched Specimen		——	——	Shear Type
LA 27			58.2	——	
LA 28			59.3	——	
LA 30			59.7	——	
LA 35			60.1	——	
LA 36			57.8	——	

* Values calculated under the assumption that stress distribution in a sectional area is uniform

** Values on the surface of a specimen

Table 3. Tensile Test Results

Specimen NO.	Wall Thickness (t mm)	Ratio of Inner Diameter to Outer Diameter (D_2/D_1)	Fracture Stress* (σ kg/mm^2)	Reduction in Area (ε)	Fracture Type
LA 50	1.0	0.8	103.8	0.328	Cleavage Type
LA 54	5.0	0	105.3	0.352	Cleavage Type
LA 62			105.7	0.360	
LA 65			108.5	0.389	
LA 70	Notched Specimen		58.3	0.013	Cleavage Type
LA 71			68.1	0.013	
LA 72			65.0	0.013	

* Values calculated under the assumption that stress distribution in a sectional area is uniform

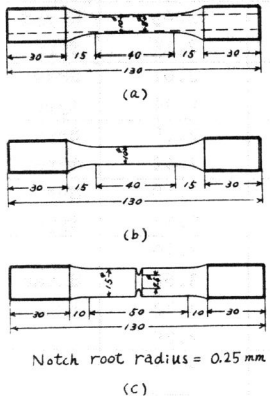

Fig. 1 Tensile specimens.

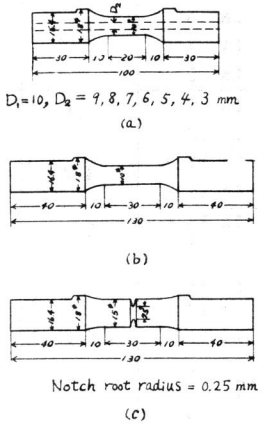

Fig. 2 Torsion specimens (L-A specimens and L-B specimens), D_1=Outer diameter, D_2=Inner diameter.

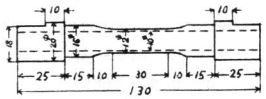

Fig. 3 Torsion specimens (M-specimens).

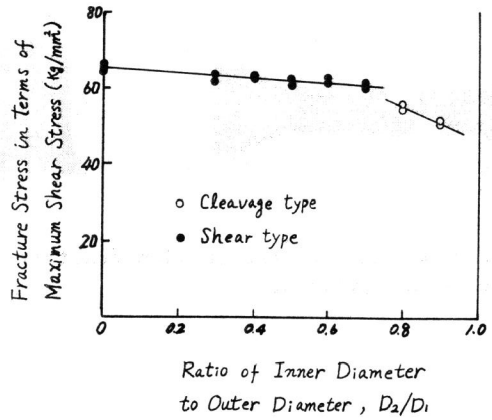

Fig. 4 The dependence of the fracture stress in terms of maximum shear stress on the ratio of the inner diameter to the outer diameter. The maximum shear stress was calculated based on the stress-strain relationship obtained from torsion tests on the solid specimens at -196°C.

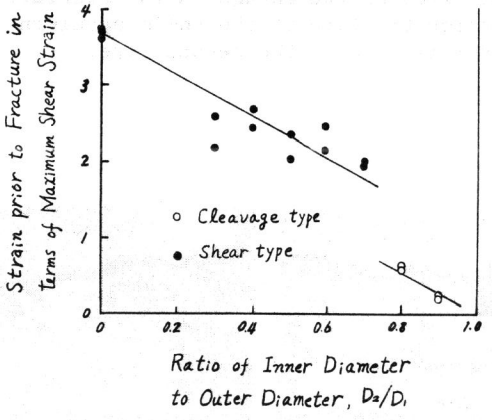

Fig. 5 The dependence of the maximum shear strain prior to fracture on the ratio of the inner diameter to the outer diameter.

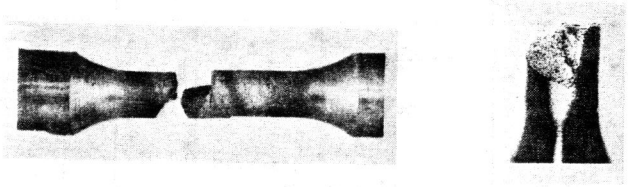

Fig. 6 The appearance of the torsion fracture surface of the solid specimen.

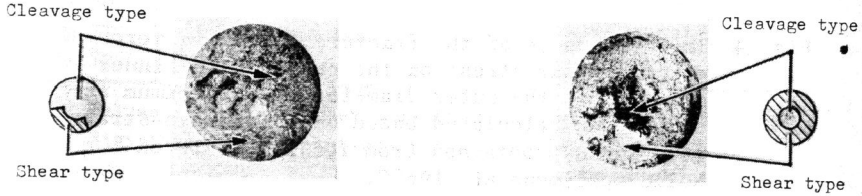

(a) The first type (b) The second type

Fig. 7 Two types of the change in the fracture mode in torsion fracture of the solid specimen. (a), the first type; (b), the second type.

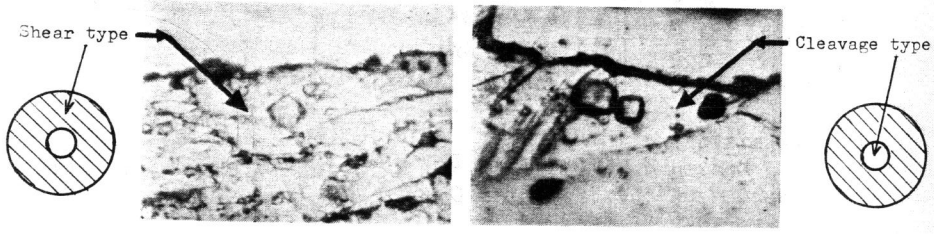

Fig. 8 Typical examples of photomicrographs of the etch pit test results. Test specimen NO.LA25.

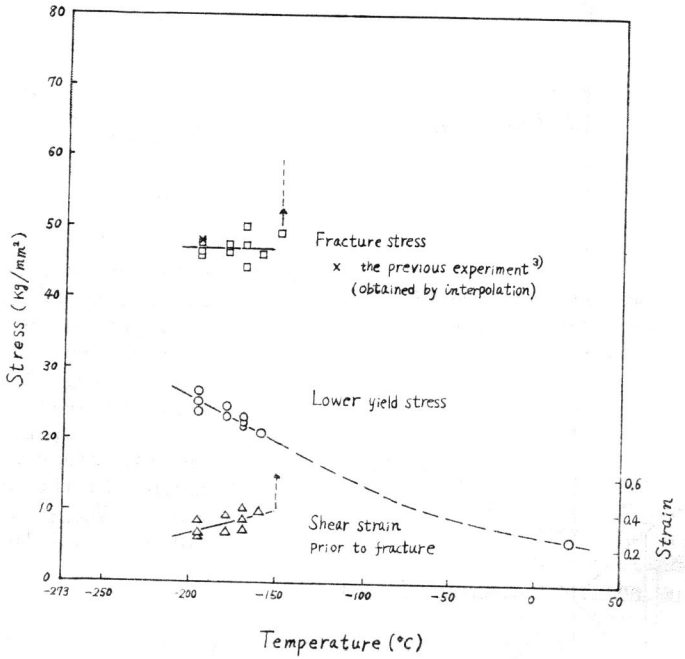

Fig. 9 The temperature dependence of the torsional fracture stress.

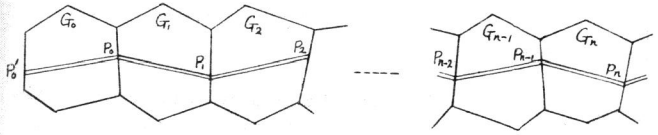

Fig.10 A model of formation of the macroscopic fracture path.

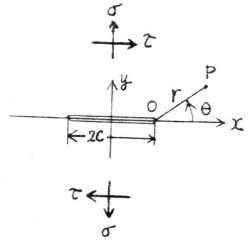

Fig.11 A slit crack subject to both normal stress and shear stress.

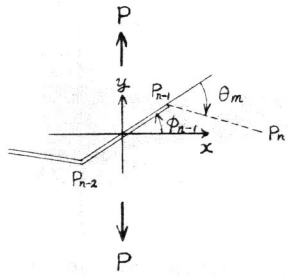

Fig.12 Crack propagation at the nth stage under uniaxial tension.

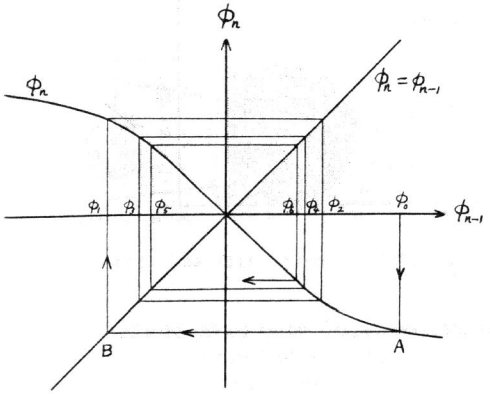

Fig.14 The graphical method of getting the direction of crack propagation.

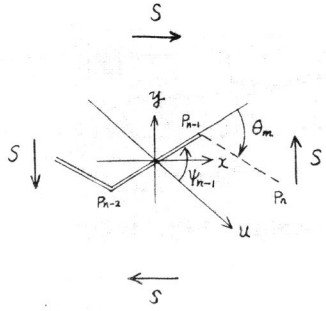

Fig.15 Crack propagation at the nth stage under simple shear.

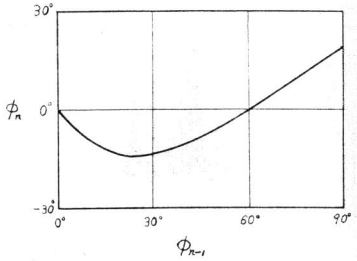

Fig.13 Relation between the directions of crack propagation under tension at two successive stages. ϕ_n is the angle between the direction of propagation at the nth stage and the normal to the specimen axis. ϕ_{n-1} is that for the (n-1)th stage.

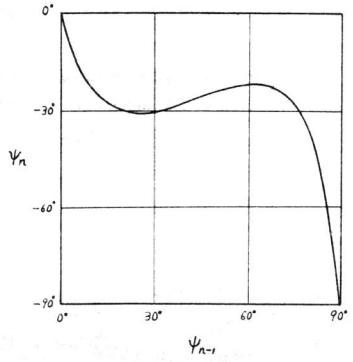

Fig.16 Relation between the direction of crack propagation under torsion at two successive stages. ψ_n is the angle between the direction of propagation at the nth stage and the direction making 45° with the specimen axis. ψ_{n-1} is that for the (n-1)th stage.

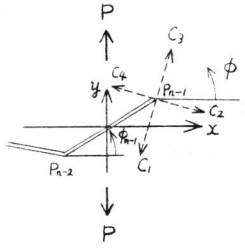

Fig.17 Cleavage planes at the crack tip in two-dimensional treatment.

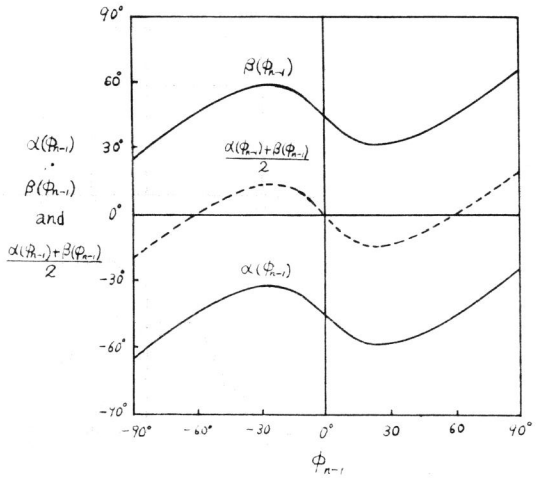

Fig.18 Possible directions of crack propagation under tension. When the angle between the direction of propagation at the (n-1)th stage and the normal to the specimen axis is ϕ_{n-1}, that for the nth stage is restricted in the region $\alpha(\phi_{n-1}) < \phi < \beta(\phi_{n-1})$.

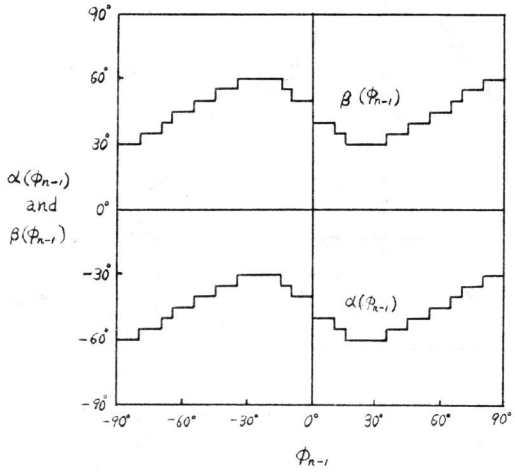

Fig.19 Approximation of $\alpha(\phi_{n-1})$ and $\beta(\phi_{n-1})$ in Fig.18.

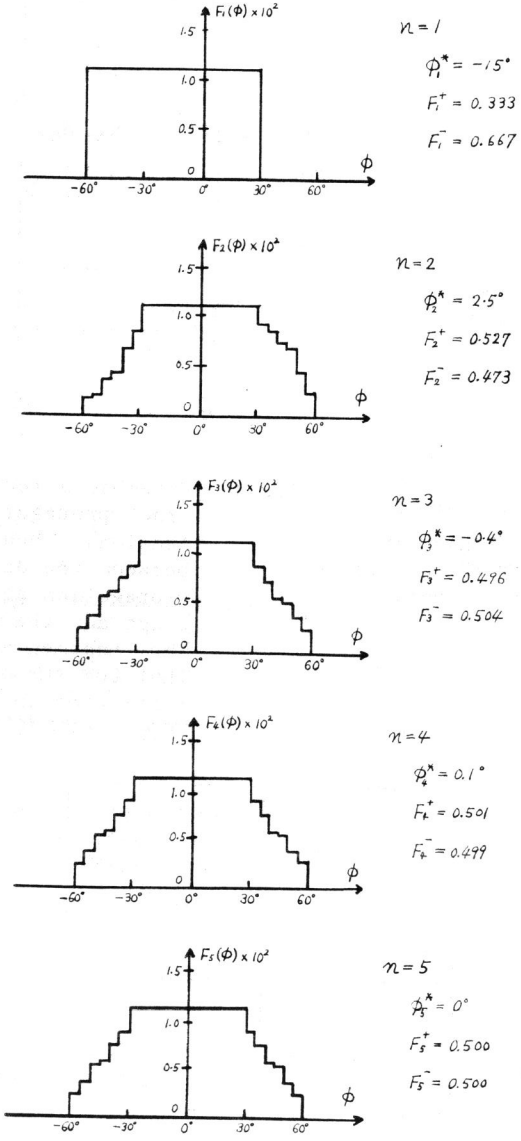

Fig.20 Change of the probability density function $Fn(\phi)$ and the mean value ϕ_n^* of the direction of crack propagation under tension with the number of stage n for $\phi_o = 22.5^\circ$. $Fn(\phi)$ and ϕ_n^* for $n \geq 6$ are the same as $F_5(\phi)$ and ϕ_5^* respectively.

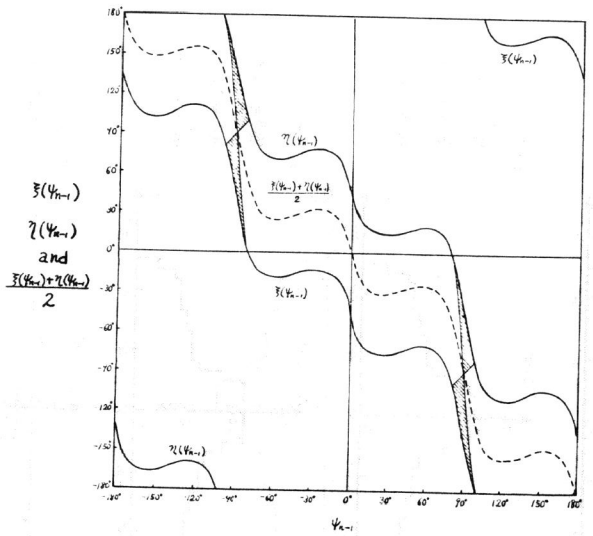

Fig.21 Possible directions of crack propagation under torsion. When the angle between the direction of propagation at the (n-1)th stage and the direction making 45° with the specimen axis is ψ_{n-1}, that for the nth stage is restricted in the region $\xi(\psi_{n-1}) < \psi < \eta(\psi_{n-1})$.

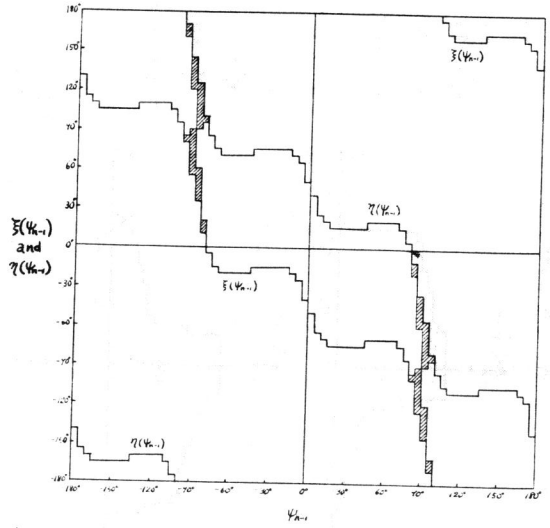

Fig.22 Approximation of $\xi(\psi_{n-1})$ and $\eta(\psi_{n-1})$ in Fig.21.

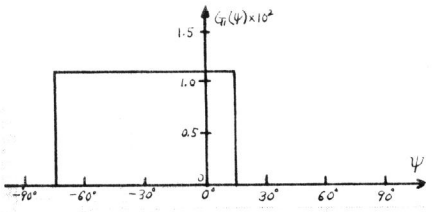

$n=1$

$\psi_1^* = -30.0°$

$G_1^+ = 0.167$

$G_1^- = 0.833$

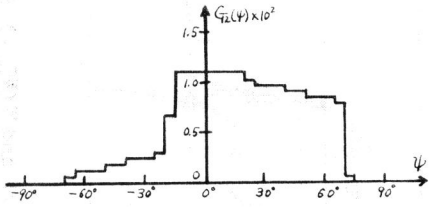

$n=2$

$\psi_2^* = 18.6°$

$G_2^+ = 0.707$

$G_2^- = 0.293$

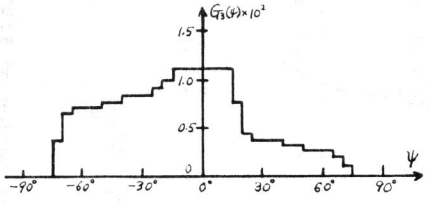

$n=3$

$\psi_3^* = -11.6°$

$G_3^+ = 0.371$

$G_3^- = 0.629$

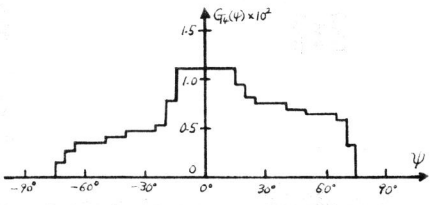

$n=4$

$\psi_4^* = 7.1°$

$G_4^+ = 0.578$

$G_4^- = 0.422$

Fig. 23 – 1

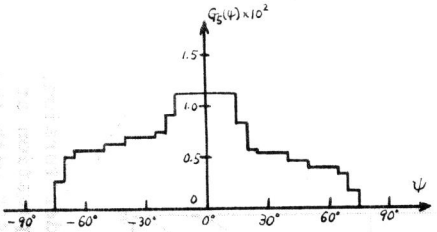

$n=5$

$\psi_5^* = -4.4°$

$G_5^+ = 0.452$

$G_5^- = 0.548$

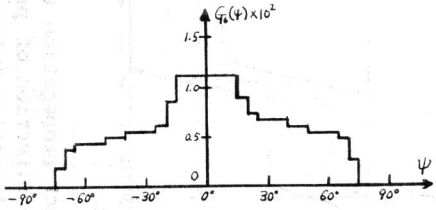

$n=6$

$\psi_6^* = 2.6°$

$G_6^+ = 0.529$

$G_6^- = 0.471$

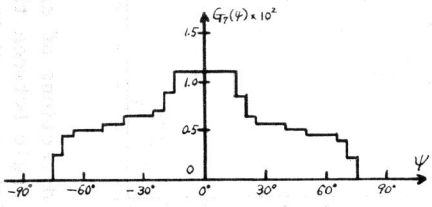

$n=7$

$\psi_7^* = -1.7°$

$G_7^+ = 0.481$

$G_7^- = 0.519$

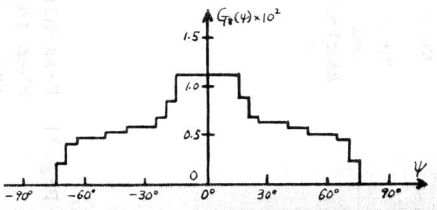

$n=8$

$\psi_8^* = 1.0°$

$G_8^+ = 0.511$

$G_8^- = 0.489$

Fig. 23 – 2

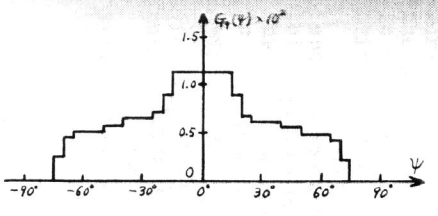

$n=9$

$\psi_9^* = -0.6°$

$G_9^+ = 0.493$

$G_9^- = 0.507$

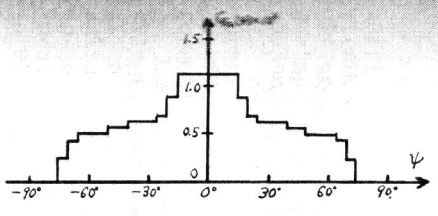

$n=12$

$\psi_{12}^* = 0.1°$

$G_{12}^+ = 0.5005$

$G_{12}^- = 0.4995$

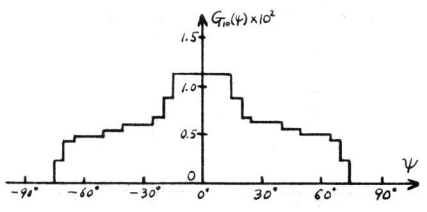

$n=10$

$\psi_{10}^* = 0.5°$

$G_{10}^+ = 0.505$

$G_{10}^- = 0.495$

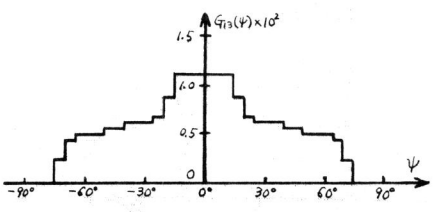

$n=13$

$\psi_{13}^* = 0°$

$G_{13}^+ = 0.500$

$G_{13}^- = 0.500$

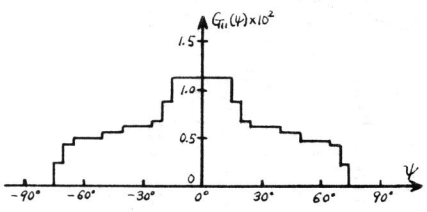

$n=11$

$\psi_{11}^* = -0.3°$

$G_{11}^+ = 0.498$

$G_{11}^- = 0.502$

Fig. 23 – 3

Fig.23 Change of the probability density function $G_n(\psi)$ and the mean value ψ_n^* of the direction of crack propagation under torsion with the number of stage n for $\psi_0 = 22.5°$. $G_n(\psi)$ and ψ_n^* for $n \geq 14$ are the same as $G_{13}(\psi)$ and ψ_{13}^* respectively.

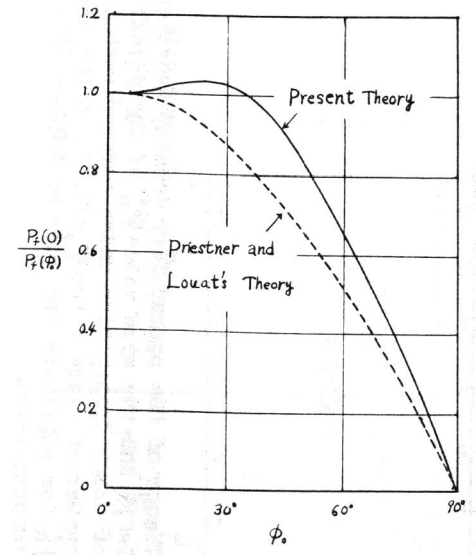

Fig.24 The dependence of the microcrack strength $P_f(\phi_0)$ on the orientation of it under uni-axial tension. ϕ_0 is the angle between an initial microcrack and the normal to the specimen axis.

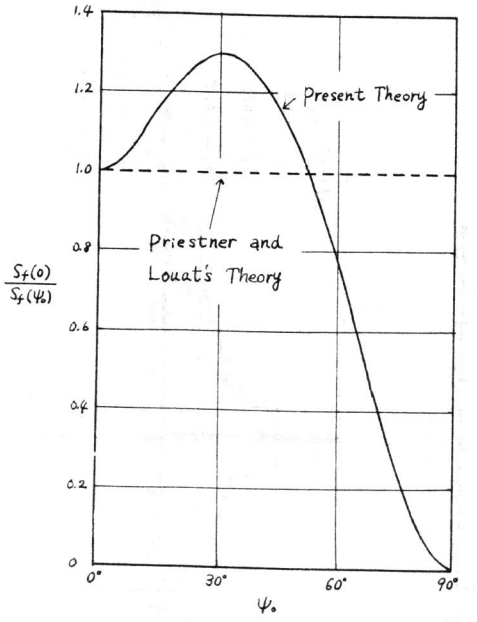

Fig.25 The dependence of the microcrack strength $S_f(\psi_0)$ on the orientation of it under torsion. ψ_0 is the angle between an initial microcrack and the direction making 45° with the specimen axis.